CASL
A DOE Energy Innovation Hub

CASL-U-2015-0223-000

Stability of Monte Carlo k-Eigenvalue Simulations with CMFD Feedback

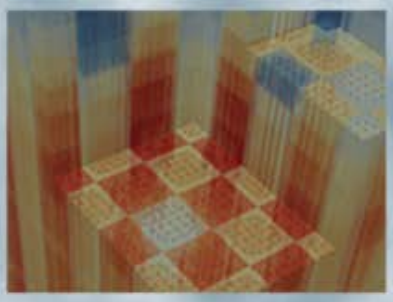

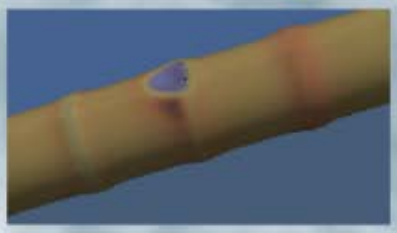

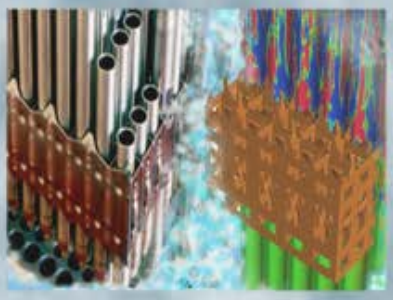

Kendra P. Keady and
Edward W. Larsen
University of Michigan

May 28, 2015

U.S. DEPARTMENT OF ENERGY | Nuclear Energy

Stability of Monte Carlo k-Eigenvalue Simulations with CMFD Feedback

Kendra P. Keady[a], Edward W. Larsen[a,*]

[a] *University of Michigan Department of Nuclear Engineering and Radiological Sciences*
2355 Bonisteel Blvd.
Ann Arbor, MI 48109

Abstract

In this paper, we perform a Fourier stability analysis of a hybrid Monte Carlo k-eigenvalue method using coarse mesh finite difference (CMFD) feedback. This method, which we call "MC-CMFD," has been discussed in several recent publications [1, 2, 3, 4, 5, 6]. The MC-CMFD method is nonlinear and contains random statistical errors; both of these features are inconsistent with the direct application of a Fourier stability analysis. To accomplish this analysis, we first formulate a non-random iteration method that approximates MC-CMFD, by assuming an infinite number of Monte Carlo particles per cycle. Then we (i) linearize this method, and (ii) Fourier-analyze the linearized method to theoretically predict its convergence properties. Finally, we demonstrate by direct numerical simulations that the Fourier analysis of the linearized non-random method accurately predicts the stability and fission source convergence rate (during the inactive cycles) of the original nonlinear MC-CMFD method. We do this by comparing the predictions of the Fourier analysis to simulations that utilize (i) a high-fidelity S_N-CMFD code (which has no random statistical errors), and (ii) a MC-CMFD code (which has random statistical errors). The Fourier analysis and our two test codes confirm that the MC-CMFD method is stable if the optical thickness of the coarse grid (in the low-order CMFD calculation) is sufficiently small. However, the spectral radius increases monotonically

*Corresponding author: Email, edlarsen@umich.edu; Phone, +1 (734) 936-0124.

CASL-U-2015-0223-000

with the coarse grid size, and if the latter exceeds a critical value, the MC-CMFD method becomes unstable. We discuss some implications of our results for practical MC-CMFD simulations.

Keywords: Neutron Transport, Hybrid Methods, Fourier Analysis, k-Eigenvalue

---

1. Introduction

Typical Monte Carlo reactor core k-eigenvalue simulations are large and complex, requiring many "inactive cycles" to converge the fission source. In a 2009 publication, a hybrid Monte Carlo method was proposed in which the fission source convergence is "accelerated" at the end of each inactive Monte Carlo cycle using the results of a discrete low-order CMFD equation [1]. This method has since been implemented and tested in a handful of codes, with mixed results [2, 3, 4, 5, 6]. In the present paper, we use a Fourier analysis to study the stability of a non-random version of this method (obtained, in effect, by assuming an infinite number of Monte Carlo particles per cycle).

Considerable prior work has utilized Fourier analysis to study the iterative convergence of iterative methods for solving fixed-source problems [7, 8]. This earlier work included the analysis of nonlinear methods, such as CMFD [8, 9, 10]. In such analyses, the original nonlinear method is first *linearized*, and then the linearized method is Fourier-analyzed. In all cases discussed in the literature, the original nonlinear iterative methods are sufficiently robust that the linearized version of the method has nearly the same convergence properties as the original nonlinear method. Thus, predicting (via Fourier analysis) the stability and efficiency of the linearized method accurately predicts the stability and efficiency of the original nonlinear method.

Also, Fourier analysis has only been used to study the stability of linear iterative schemes for deterministic problems. It is not known how to include statistical noise in a Fourier stability analysis. Thus, to accomplish the work outlined in this paper, we analyze a non-random version of the MC-CMFD method,

obtained by (mathematically) assuming an infinite number of Monte Carlo particles per cycle. This "non-random MC-CMFD" method has a straightforward mathematical formulation, which can be linearized and then Fourier-analyzed.

To our knowledge, only one previous publication, by S.G. Hong, K.-S. Kim, and J.S. Song, has addressed the Fourier-analysis of iterative methods for k-eigenvalue problems [11] – and that prior work considered only iterative methods for deterministic simulations. (The iteration processes for deterministic and hybrid Monte Carlo k-eigenvalue simulations are related, but different.) We are particularly interested in the effect on stability of the optical thickness of a coarse mesh in MC-CMFD simulations [5]. The work in the present paper has little direct overlap with the previous work in [11].

We emphasize that our Fourier analysis is only valid for the hypothetical non-random MC-CMFD method having an infinite number of Monte Carlo particles per cycle. While this idealized method cannot be simulated in practice, the infinite-particle Fourier analysis predicts a "best-case" convergence rate for the real method with a finite number of particles. If the MC-CMFD method is unstable in the non-random infinite-particle limit, it cannot be expected to be stable for a practical simulation with a finite number of particles per cycle. In fact, we observe in our numerical experiments that if the non-random MC-CMFD method has a spectral radius less than but sufficiently close to unity, then a "fixed" amount of random noise per cycle can actually drive the random MC-CMFD method unstable. Therefore, again, the results of the Fourier analysis represent a "best-case" convergence rate.

Also, the Fourier analysis of the non-random MC-CMFD method only describes the convergence properties of the MC-CMFD method during inactive cycles, when the error in the fission source is greater than the random statistical error. During active cycles, when the error in the fission source is dominated by random statistical fluctuations, the Fourier analysis is not relevant.

Not surprisingly, we find that for non-random MC-CMFD, reducing the size of the coarse mesh reduces the spectral radius and improves the stability of the method. (The same is basically true for fixed-source CMFD problems

[8].) We also find that if the coarse mesh exceeds a critical optical thickness, the non-random MC-CMFD method becomes unstable. (This is also true for fixed-source problems with sufficiently high scattering ratios [8].) Since the deterministic CMFD and MC-CMFD methods differ, their stability properties differ for a specified coarse mesh thickness. Nonetheless, for both methods (with a sufficiently high scattering ratio for deterministic CMFD), the following basic trends are the same: the spectral radius (i) is less than unity for small coarse mesh thicknesses, (ii) monotonically increases as the coarse mesh width increases, and (iii) exceeds unity when the coarse mesh width exceeds a critical value.

In the present paper we derive theoretical predictions for the spectral radius ρ of the non-random MC-CMFD method as a function of the coarse mesh size. We include comparisons with direct numerical simulations, demonstrating that the theoretical predictions are accurate. Our numerical demonstrations include (i) a finite-differenced S_N code, especially written to simulate the non-random MC-CMFD method, and (ii) a hybrid MC-CMFD code using a large (but not infinite!) number of Monte Carlo particles per cycle. Our results show that the non-random CMFD method is stable when the optical thickness of a coarse grid cell (in the low-order CMFD calculation) is small. However, the spectral radius of the non-random MC-CMFD method increases as the optical thickness of the coarse grid cells increases, to the point where the former exceeds unity when the latter exceeds a critical value. (At this point, the non-random MC-CMFD method becomes unstable.) In all cases, the Fourier analysis and the finite-differenced S_N code produced nearly identical estimates of ρ.

The comparisons between the Fourier analysis and the MC-CMFD code were less close, due the the effects of statistical noise. However, for problems in which $0.5 < \rho < 0.98$, very good agreement was seen. (For problems with $\rho < 0.5$, convergence was so rapid that with statistical noise, it was very difficult to obtain accurate Monte Carlo estimates of ρ. Similarly, with $\rho > 0.98$, we found that a small amount of noise can drive an otherwise "barely stable" configuration unstable).

Overall, the Fourier analysis accurately predicts the rate of convergence (or divergence) of the fission source in MC-CMFD problems during inactive cycles, when the error in the fission source exceeds the random statistical errors. If the non-random MC-CMFD method is unstable for a particular set of parameters, then surely it would be unwise to employ this method using the same parameters with a finite number of particles per cycle. We are not aware of any previously-published work that addresses the issue of numerical instabilities in MC-CMFD simulations.

A lesson for more general computational methods can be gleaned from the work presented in this paper. It is well-known that iterative methods for deterministic methods can be unstable, due to inherent properties of the mathematical equations that describe the method. It is also well-known that Monte Carlo methods have statistical errors, which can usually be controlled by using a sufficiently large number of trials. This paper shows that hybrid methods – which combine elements of both Monte Carlo and deterministic methods – can suffer from both statistical errors and fundamental instabilities, and that instabilities can occur even if the number of Monte Carlo particles used is (hypothetically) infinite.

The remainder of this paper is organized as follows. In Section II, the non-linear non-random MC-CMFD iteration strategy for k-eigenvalue problems is described. In Section III, this method is linearized, and in Section IV, the continuous linearized strategy is approximated by a discrete problem and Fourier-analyzed.

In Section V, the the Fourier analysis Section IV is employed to predict the stability and convergence of the MC-CMFD method, and comparisons are made with independent deterministic and Monte Carlo test codes. Our results confirm the accuracy of the Fourier analysis predictions. The paper concludes in Section VI with a discussion on the implications of this work for practical MC-CMFD simulations, and possible extensions of the results for more general problems.

2. CMFD Iteration Strategy for Monte Carlo *k*-Eigenvalue Problems

Here we describe the non-random MC-CMFD iteration strategy for solving Monte Carlo k-eigenvalue problems. (This method is simply the MC-CMFD method [1], assuming an infinite number of particles per cycle.) We consider the following one-group, planar-geometry k-eigenvalue problem on the domain $0 \leq x \leq X$ with periodic boundary conditions:

$$\mu \frac{d}{dx}\psi(x,\mu) + \Sigma_t \psi(x,\mu) - \frac{\Sigma_s}{2}\phi(x) = \frac{\nu\Sigma_f}{2k}\phi(x) \ , \quad 0 \leq x \leq X \ , \ \ -1 \leq \mu \leq 1 \ , \tag{1a}$$

$$\psi(0,\mu) = \psi(X,\mu) \ , \ \ -1 \leq \mu \leq 1 \ , \tag{1b}$$

where

$$\phi(x) = \int_{-1}^{1} \psi(x,\mu) d\mu \ . \tag{1c}$$

The l^{th} MC-CMFD iteration (or "cycle") begins with Eqs. (1), written with iteration superscripts as follows:

$$\mu \frac{d}{dx}\psi^{(l+1/2)}(x,\mu) + \Sigma_t \psi^{(l+1/2)}(x,\mu) - \frac{\Sigma_s}{2}\phi^{(l+1/2)}(x) = \frac{\nu\Sigma_f}{2k^{(l)}}\phi^{(l)}(x) \ , \quad 0 \leq x \leq X \ , \ \ -1 \leq \mu \leq 1 \ , \tag{2a}$$

$$\psi^{(l+1/2)}(0,\mu) = \psi^{(l+1/2)}(X,\mu) \ , \ \ -1 \leq \mu \leq 1 \ , \tag{2b}$$

where

$$\phi^{(l+1/2)}(x) = \int_{-1}^{1} \psi^{(l+1/2)}(x,\mu) d\mu \ . \tag{2c}$$

In contrast to standard deterministic methods, the Monte Carlo transport simulation shown in Eq. (2a) treats scattering *implicitly*; the scattering source is treated as being fully converged, because Monte Carlo methods simulate full particle histories (from birth until death) within each cycle. Eqs. (2) are not discretized in space or angle, because Monte Carlo simulations involve no such discretizations. Finally, Eqs. (2) have no terms that describe random errors. These equations apply to Monte Carlo simulations only in the limit in which

the number of particles per cycle is sufficiently large that statistical errors can be ignored.

To proceed, we impose a "coarse" spatial grid on the system, with J cells of width Δ_j ($1 \leq j \leq J$). During the solution of Eqs. (2), the following quantities are tallied on the coarse grid for $1 \leq j \leq J$. (Capital letters (Φ, Δ) denote coarse-grid quantities, while lower-case letters (ψ, ϕ) denote continuous quantities.)

$$\Phi_j^{(l+1/2)} = \frac{1}{\Delta_j} \int_{x_{j-1/2}}^{x_{j+1/2}} \phi^{(l+1/2)}(x)dx \;, \tag{3a}$$

$$\Phi_{1,j\pm1/2}^{(l+1/2)} = \int_{-1}^{1} \mu\psi^{(l+1/2)}(x_{j\pm1/2},\mu)d\mu \;, \tag{3b}$$

$$\Sigma_{a,j}^{(l+1/2)} = \frac{\int_{x_{j-1/2}}^{x_{j+1/2}} \Sigma_a(x)\phi^{(l+1/2)}(x)dx}{\int_{x_{j-1/2}}^{x_{j+1/2}} \phi^{(l+1/2)}(x)dx} \;, \tag{3c}$$

$$\Sigma_{t,j}^{(l+1/2)} = \frac{\int_{x_{j-1/2}}^{x_{j+1/2}} \Sigma_t(x)\phi^{(l+1/2)}(x)dx}{\int_{x_{j-1/2}}^{x_{j+1/2}} \phi^{(l+1/2)}(x)dx} \;, \tag{3d}$$

$$\nu\Sigma_{f,j}^{(l+1/2)} = \frac{\int_{x_{j-1/2}}^{x_{j+1/2}} \nu\Sigma_f(x)\phi^{(l+1/2)}(x)dx}{\int_{x_{j-1/2}}^{x_{j+1/2}} \phi^{(l+1/2)}(x)dx} \;. \tag{3e}$$

Also, the following interior-edge quantities are calculated:

$$\tilde{D}_{j+1/2}^{(l+1/2)} = \frac{2}{3}\left(\frac{1}{\Sigma_{t,j}^{(l+1/2)}\Delta_j + \Sigma_{t,j+1}^{(l+1/2)}\Delta_{j+1}}\right) \;, \tag{3f}$$

$$\hat{D}_{j+1/2}^{(l+1/2)} = \frac{\Phi_{1,j+1/2}^{(l+1/2)} + \tilde{D}_{j+1/2}^{(l+1/2)}(\Phi_{j+1}^{(l+1/2)} - \Phi_j^{(l+1/2)})}{\Phi_{j+1}^{(l+1/2)} + \Phi_j^{(l+1/2)}} \;, \tag{3g}$$

and the exterior edge quantities are calculated using the periodic boundary condition:

$$\begin{aligned}\tilde{D}_{1/2}^{(l+1/2)} &= \tilde{D}_{J+1/2}^{(l+1/2)} \\ &= \frac{2}{3}\left(\frac{1}{\Sigma_{t,1}^{(l+1/2)}\Delta_1 + \Sigma_{t,J}^{(l+1/2)}\Delta_J}\right) \;,\end{aligned} \tag{3h}$$

$$\begin{aligned}\hat{D}_{1/2}^{(l+1/2)} &= \hat{D}_{J+1/2}^{(l+1/2)} \\ &= \frac{\Phi_{1,1/2}^{(l+1/2)} + \tilde{D}_{1/2}^{(l+1/2)}(\Phi_1^{(l+1/2)} - \Phi_J^{(l+1/2)})}{\Phi_1^{(l+1/2)} + \Phi_J^{(l+1/2)}} \;.\end{aligned} \tag{3i}$$

The Monte Carlo estimates of $\Sigma_{a,j}^{(l+1/2)}$, $\nu\Sigma_{f,j}^{(l+1/2)}$, $\hat{D}_{j+1/2}^{(l+1/2)}$, and $\tilde{D}_{j+1/2}^{(l+1/2)}$ are used to build the coefficients of the CMFD system. The low-order discrete CMFD equations take the form:

$$\Phi_{1,j+1/2}^{(l+1)} - \Phi_{1,j-1/2}^{(l+1)} + \Sigma_{a,j}^{(l+1/2)}\Phi_j^{(l+1)}\Delta_j = \frac{\nu\Sigma_{f,j}^{(l+1/2)}}{k^{(l+1)}}\Phi_j^{(l+1)}\Delta_j \ , \ \ 1 \le j \le J \ , \tag{4a}$$

$$\Phi_{1,j+1/2}^{(l+1)} = \tilde{D}_{j+1/2}^{(l+1/2)}(\Phi_{j+1}^{(l+1)} - \Phi_j^{(l+1)}) + \hat{D}_{j+1/2}^{(l+1/2)}(\Phi_{j+1}^{(l+1)} + \Phi_j^{(l+1)}) \ , \tag{4b}$$

$$\Phi_{1,1/2}^{(l+1)} = \Phi_{1,J+1/2}^{(l+1)} \ , \tag{4c}$$

$$1 = \frac{1}{J}\sum_{j=1}^{J}\Phi_j^{(l+1)} \ . \tag{4d}$$

On convergence, Eq. (4a) is simply the *neutron balance equation*, obtained by integrating Eq. (1a) over angle and the j^{th} coarse cell. Also on convergence, Eq. (4b) reduces to the identity $\Phi_{1,j+1/2} = \Phi_{1,j+1/2}$. (The motivation behind the specific construction of Eq. (4b) is Fick's Law.) Finally, on convergence Eq. (4c) reduces to the condition from Eq. (1b) that the converged scalar flux must be periodic. For these reasons, the low-order discrete Eqs. (4) are fully consistent with the high-order continuous Eqs. (1), and on convergence, the solution of these equations would be the true scalar fluxes, volume-averaged over each coarse cell.

To proceed, the "current" terms $\Phi_{1,j+1/2}^{(l+1)}$ in Eqs. (4a) and (4b) are eliminated to form an algebraic system involving only the coarse-grid scalar fluxes, $\Phi_j^{(l+1)}$ (this system is not tridiagonal because of the periodic boundary condition). The solution of Eqs. (4) yields a new estimate of the k-eigenvalue and coarse-grid scalar flux, the latter of which is used to scale the continuous fine-grid fission source for the next cycle:

$$\phi^{(l+1)}(x) = \phi^{(l+1/2)}(x)\left[\frac{\Phi_j^{(l+1)}}{\Phi_j^{(l+1/2)}}\right] \ , \ \ x_{j-1/2} \le x \le x_{j+1/2} \ , \ \ 1 \le j \le J \ . \tag{5}$$

This completes the description of the MC-CMFD iteration strategy [1]. To summarize, a single iteration "cycle" has the following steps: (i) perform a Monte Carlo calculation, using the previous-cycle estimate of the fission source term (or initial guess if $l = 0$) [Eqs. (2)], (ii) use Monte Carlo tallies to form the coefficients of the CMFD system [Eqs. (3)], (iii) solve the CMFD system [Eqs. (4)] to obtain an updated estimate of the coarse-grid scalar flux and eigenvalue, and (iv) scale the fine-grid fission source using the updated coarse-grid scalar flux [Eq. (5)]. If the number of Monte Carlo particles is allowed to limit to ∞, then the preceding equations mathematically define the "non-random MC-CMFD" method, which we will next linearize, and then Fourier-analyze.

3. Linearized Non-Random MC-CMFD Method

To linearize the non-random MC-CMFD k-eigenvalue iteration method defined above, we consider a special problem in which the exact eigenfunction is constant (independent of space and angle). Specifically, we consider a spatially uniform system with periodic boundary conditions:

$$\mu\frac{d}{dx}\psi^{(l+1/2)}(x,\mu)+\Sigma_t\psi^{(l+1/2)}(x,\mu)-\frac{\Sigma_s}{2}\phi^{(l+1/2)}(x)=\frac{\nu\Sigma_f}{2k^{(l)}}\phi^{(l)}(x)\;, \tag{6a}$$

$$0\le x\le X\;,\;\;-1\le\mu\le 1\;,$$

$$\psi^{(l+1/2)}(0,\mu)=\psi^{(l+1/2)}(X,\mu)\;,\;\;-1\le\mu\le 1\;. \tag{6b}$$

The CMFD grid is assumed to be uniform, with J cells of width Δ. The coarse-grid cross sections and diffusivities ($\tilde{D}$) are known exactly:

$$\Sigma_{a,j}^{(l+1/2)}=\Sigma_a\;, \tag{7a}$$

$$\Sigma_{t,j}^{(l+1/2)}=\Sigma_t\;, \tag{7b}$$

$$\nu\Sigma_{f,j}^{(l+1/2)}=\nu\Sigma_f\;, \tag{7c}$$

$$\tilde{D}_{j+1/2}^{(l+1/2)}=\tilde{D}=\frac{1}{3\Sigma_t\Delta}\;, \tag{7d}$$

while the remainder of the equations become:

$$\phi^{(l+1/2)}(x)=\int_{-1}^{1}\psi^{(l+1/2)}(x,\mu)d\mu\;, \tag{8a}$$

$$\Phi_j^{(l+1/2)} = \frac{1}{\Delta}\int_{x_{j-1/2}}^{x_{j+1/2}}\int_{-1}^{1}\psi^{(l+1/2)}(x,\mu)d\mu dx\ , \tag{8b}$$

$$\Phi_{1,j+1/2}^{(l+1/2)} = \int_{-1}^{1}\mu\psi^{(l+1/2)}(x_{j+1/2},\mu)d\mu\ , \tag{8c}$$

$$\hat{D}_{j+1/2}^{(l+1/2)} = \frac{\Phi_{1,j+1/2}^{(l+1/2)} + \tilde{D}(\Phi_{j+1}^{(l+1/2)} - \Phi_j^{(l+1/2)})}{\Phi_{j+1}^{(l+1/2)} + \Phi_j^{(l+1/2)}}\ , \tag{8d}$$

$$\Phi_{1,j+1/2}^{(l+1)} - \Phi_{1,j-1/2}^{(l+1)} + \Sigma_a\Phi_j^{(l+1)}\Delta = \frac{\nu\Sigma_f}{k^{(l+1)}}\Phi_j^{(l+1)}\Delta\ ,\ \ 1 \le j \le J\ , \tag{8e}$$

$$\Phi_{1,j+1/2}^{(l+1)} = \tilde{D}(\Phi_{j+1}^{(l+1)} - \Phi_j^{(l+1)}) + \hat{D}_{j+1/2}^{(l+1/2)}(\Phi_{j+1}^{(l+1)} + \Phi_j^{(l+1)})\ , \tag{8f}$$

$$\Phi_{1,1/2}^{(l+1/2)} = \Phi_{1,J+1/2}^{(l+1/2)}\ , \tag{8g}$$

$$1 = \frac{1}{J}\sum_{j=1}^{J}\Phi_j^{(l+1)}\ . \tag{8h}$$

On convergence, this problem has the following exact solution:

$$\psi(x,\mu) = \frac{1}{2}\ , \tag{9a}$$

$$\Phi_j = \phi(x) = 1\ , \tag{9b}$$

$$\Phi_{1,j+1/2} = 0\ , \tag{9c}$$

$$k = \frac{\nu\Sigma_f}{\Sigma_a}\ . \tag{9d}$$

To proceed, we define the following linear expansions around the exact solution (with $\epsilon \ll 1$):

$$\psi^{(l+1/2)}(x,\mu) = \frac{1}{2} + \epsilon\tilde{\psi}^{(l+1/2)}(x,\mu)\ , \tag{10a}$$

$$\phi^{(l+1/2)}(x) = 1 + \epsilon\tilde{\phi}^{(l+1/2)}(x)\ , \tag{10b}$$

$$\phi^{(l+1)}(x) = 1 + \epsilon\tilde{\phi}^{(l+1)}(x)\ , \tag{10c}$$

$$\Phi_j^{(l+1/2)} = 1 + \epsilon\tilde{\Phi}_j^{(l+1/2)}\ , \tag{10d}$$

$$\Phi_j^{(l+1)} = 1 + \epsilon\tilde{\Phi}_j^{(l+1)}\ , \tag{10e}$$

$$\Phi_{1,j+1/2}^{(l+1/2)} = 0 + \epsilon\tilde{\Phi}_{1,j+1/2}^{(l+1/2)}\ , \tag{10f}$$

$$\Phi_{1,j+1/2}^{(l+1)} = 0 + \epsilon\tilde{\Phi}_{1,j+1/2}^{(l+1)} \,, \tag{10g}$$

$$\hat{D}_{j+1/2}^{(l+1/2)} = 0 + \epsilon\hat{d}_{j+1/2}^{(l+1/2)} \,, \tag{10h}$$

$$\frac{1}{k^{(l+1)}} = \frac{\Sigma_a}{\nu\Sigma_f} + \epsilon\delta^{(l+1)} \,. \tag{10i}$$

Since the coarse-grid cross sections and diffusion coefficients are known exactly, these quantities are not expanded. Inserting Eqs. (10) into Eqs. (6) and (8), and equating $O(\epsilon)$ terms, we obtain:

$$\mu\frac{d}{dx}\tilde{\psi}^{(l+1/2)}(x,\mu)+\Sigma_t\tilde{\psi}^{(l+1/2)}(x,\mu) - \frac{\Sigma_s}{2}\tilde{\phi}^{(l+1/2)}(x) = \frac{\nu\Sigma_f}{2}\delta^{(l)} + \frac{\Sigma_a}{2}\tilde{\phi}^{(l)}(x) \,, \tag{11a}$$

$$0 \le x \le X \,, \;\; -1 \le \mu \le 1 \,,$$

$$\tilde{\psi}^{(l+1/2)}(0,\mu) = \tilde{\psi}^{(l+1/2)}(X,\mu) \,, \;\; -1 \le \mu \le 1 \,, \tag{11b}$$

$$\tilde{\phi}^{(l+1/2)}(x) = \int_{-1}^{1} \tilde{\psi}^{(l+1/2)}(x,\mu)d\mu \,, \tag{11c}$$

$$\tilde{\Phi}_{j}^{(l+1/2)} = \frac{1}{\Delta}\int_{x_{j-1/2}}^{x_{j+1/2}}\int_{-1}^{1} \tilde{\psi}^{(l+1/2)}(x,\mu)d\mu dx \,, \tag{11d}$$

$$\tilde{\Phi}_{1,j+1/2}^{(l+1/2)} = \int_{-1}^{1} \mu\tilde{\psi}^{(l+1/2)}(x_{j+1/2},\mu)d\mu \,, \tag{11e}$$

$$\hat{d}_{j+1/2}^{(l+1/2)} = \frac{1}{2}(\tilde{\Phi}_{1,j+1/2}^{(l+1/2)} + \tilde{D}(\tilde{\Phi}_{j+1}^{(l+1/2)} - \tilde{\Phi}_{j}^{(l+1/2)})) \,, \tag{11f}$$

$$\nu\Sigma_f\delta^{(l+1)}\Delta = (\tilde{\Phi}_{1,j+1/2}^{(l+1)} - \tilde{\Phi}_{1,j-1/2}^{(l+1)}) \,, \tag{11g}$$

$$\tilde{\Phi}_{1,j+1/2}^{(l+1)} = -\tilde{D}(\tilde{\Phi}_{j+1}^{(l+1)} - \tilde{\Phi}_{j}^{(l+1)}) + 2\hat{d}_{j+1/2}^{(l+1/2)} \,, \tag{11h}$$

$$\tilde{\Phi}_{1,1/2}^{(l+1/2)} = \tilde{\Phi}_{1,J+1/2}^{(l+1/2)} \,, \tag{11i}$$

$$0 = \frac{1}{J}\sum_{j=1}^{J}\tilde{\Phi}_{j}^{(l+1)} \,, \tag{11j}$$

and

$$\tilde{\phi}^{(l+1)}(x) = \tilde{\phi}^{(l+1/2)}(x) + \tilde{\Phi}_{j}^{(l+1)} - \tilde{\Phi}_{j}^{(l+1/2)} \,, \tag{11k}$$

$$x_{j-1/2} \le x \le x_{j+1/2} \ , \ \ 1 \le j \le J \ .$$

We note that several of the linearized equations differ in form from Eqs. (2) - (4), because the original equations contained nonlinear terms.

After some straightforward algebra (omitted here for brevity), we find:

$$\delta^{(l+1)} = 0 \ . \tag{12}$$

This shows that the non-random MC-CMFD method converges the $O(\epsilon)$ component of the system eigenvalue after only one iteration. However, the $O(\epsilon)$ component of the eigenfunction is not converged after one iteration; the Fourier analysis predicts the rate of convergence of this component of the eigenfunction.

Inserting Eq. (12) into Eqs. (11a) and rearranging to algebraically eliminate $\hat{d}_{j+1/2}^{(l+1/2)}$, we obtain the following system of equations for the linearized non-random MC-CMFD method:

$$\mu \frac{d}{dx} \tilde{\psi}^{(l+1/2)}(x,\mu) + \Sigma_t \tilde{\psi}^{(l+1/2)}(x,\mu) - \frac{\Sigma_s}{2} \tilde{\phi}^{(l+1/2)}(x) = \frac{\Sigma_a}{2} \tilde{\phi}^{(l)}(x) \ , \tag{13a}$$

$$0 \le x \le X, -1 \le \mu \le 1 \ ,$$

$$\tilde{\psi}^{(l+1/2)}(0,\mu) = \tilde{\psi}^{(l+1/2)}(X,\mu) \ , \ \ -1 \le \mu \le 1 \ , \tag{13b}$$

$$\tilde{\phi}^{(l+1/2)}(x) = \int_{-1}^{1} \tilde{\psi}^{(l+1/2)}(x,\mu) d\mu \ , \tag{13c}$$

$$\tilde{\Phi}_j^{(l+1/2)} = \frac{1}{\Delta} \int_{x_{j-1/2}}^{x_{j+1/2}} \tilde{\phi}^{(l+1/2)}(x) dx \ , \tag{13d}$$

$$\tilde{\Phi}_{1,j+1/2}^{(l+1/2)} = \int_{-1}^{1} \mu \tilde{\psi}^{(l+1/2)}(x_{j+1/2},\mu) d\mu \ , \tag{13e}$$

$$\begin{aligned} \tilde{\Phi}_{j+1}^{(l+1)} - 2\tilde{\Phi}_j^{(l+1)} + \tilde{\Phi}_{j-1}^{(l+1)} = \frac{1}{\tilde{D}} (\tilde{\Phi}_{1,j+1/2}^{(l+1/2)} - \tilde{\Phi}_{1,j-1/2}^{(l+1/2)}) \\ + \tilde{\Phi}_{j+1}^{(l+1/2)} - 2\tilde{\Phi}_j^{(l+1/2)} + \tilde{\Phi}_{j-1}^{(l+1/2)} \ , \ \ 1 \le j \le J \ , \end{aligned} \tag{13f}$$

$$\tilde{\Phi}_1^{(l+1)} = \tilde{\Phi}_{J+1}^{(l+1)} \ , \tag{13g}$$

$$0 = \frac{1}{J} \sum_{j=1}^{J} \tilde{\Phi}_j^{(l+1)} \ , \tag{13h}$$

$$\tilde{\phi}^{(l+1)}(x) = \tilde{\phi}^{(l+1/2)}(x) + \tilde{\Phi}_j^{(l+1)} - \tilde{\Phi}_j^{(l+1/2)} \,, \qquad (13i)$$
$$x_{j-1/2} \le x \le x_{j+1/2} \,, \;\; 1 \le j \le J \,.$$

In Eqs. (13), the eigenvalue is converged exactly [Eq. (3.7)], but the eigenfunction is not converged. The Fourier analysis of the linearized equations, performed next in Section IV, determines the rate of convergence of the eigenfunction. We emphasize again that the Fourier analysis contains no terms that account for statistical errors; the analysis applies only when the statistical noise in the solution is sufficiently small that it can be ignored.

4. Fourier Analysis

To carry out the Fourier analysis, we discretize the Monte Carlo portion of the linearized system in angle and space. This is an approximation to the continuous Monte Carlo problem, but it enables us to formulate and solve a block matrix system numerically for the spectral radius. To ensure that the discrete results are accurate enough to closely approximate the original problem, we carry out a parametric study to determine an adequately fine space-angle grid (see Section V).

Thus, we approximate the Monte Carlo k-eigenvalue problem by a discrete ordinates problem formulated on a fine space-angle grid, with M discrete angles from $1 \le m \le M$ and K fine spatial cells of thickness h ($1 \le k \le K$). We use the "coarse-grid parameter" $p = \frac{\Delta}{h}$ to denote the number of fine cells per coarse cell, and we introduce the notation

$$\sum_{k \in j} (\cdot) \,, \qquad (14)$$

to describe a sum over the fine cells k belonging to coarse cell j. Also, we use Gauss-Legendre quadrature sets, which satisfy:

$$\sum_{m=1}^{M} w_m = 2 \,. \qquad (15)$$

Using this notation, the discretized version of Eq. (13a) can be written in the form:

$$\frac{\mu_m}{h}(\tilde{\psi}^{(l+1/2)}_{k+1/2,m} - \tilde{\psi}^{(l+1/2)}_{k-1/2,m}) + \Sigma_t \tilde{\psi}^{(l+1/2)}_{k,m} - \frac{\Sigma_s}{2}\tilde{\phi}^{(l+1/2)}_k = \frac{\Sigma_a}{2}\tilde{\phi}^{(l)}_k \ , \tag{16a}$$

$$1 \le m \le M, \ \ 1 \le k \le K \ ,$$

$$\tilde{\psi}^{(l+1/2)}_{1/2,m} = \tilde{\psi}^{(l+1/2)}_{K+1/2,m} \ , \ \ 1 \le m \le M \ . \tag{16b}$$

Similarly, the linearized scalar flux expression becomes:

$$\tilde{\phi}^{(l+1/2)}_k = \sum_{m=1}^{M} w_m \tilde{\psi}^{(l+1/2)}_{k,m} \ . \tag{16c}$$

To close the system, we introduce the weighted diamond auxiliary equations:

$$\tilde{\psi}^{(l+1/2)}_{k,m} = \left(\frac{1+\alpha_m}{2}\right)\tilde{\psi}^{(l+1/2)}_{k+1/2,m} + \left(\frac{1-\alpha_m}{2}\right)\tilde{\psi}^{(l+1/2)}_{k-1/2,m} \ ,$$

$$1 \le m \le M \ , \ \ 1 \le k \le K \ . \tag{16d}$$

In this work, we use the *Step Characteristic* spatial discretization, with

$$\alpha_m = \frac{1+e^{-\Sigma_t h/\mu_m}}{1-e^{-\Sigma_t h/\mu_m}} - \frac{2\mu_m}{\Sigma_t h} \ , \ \ 1 \le m \le M \ . \tag{16e}$$

The equations that "link" the Monte Carlo problem to CMFD (Eqs. (13d), (13e) and (14)) must also be discretized, while the CMFD equations themselves (Eqs. (13f) and (13g)) remain essentially unchanged:

$$\tilde{\Phi}^{(l+1/2)}_j = \frac{1}{p}\sum_{k\in j}\tilde{\phi}^{(l+1/2)}_k \ , \tag{16f}$$

$$\tilde{\Phi}^{(l+1/2)}_{1,j+1/2} = \sum_{m=1}^{M} w_m \mu_m \tilde{\psi}^{(l+1/2)}_{(jp)+1/2,m} \ , \tag{16g}$$

$$\tilde{\Phi}^{(l+1)}_{j+1} - 2\tilde{\Phi}^{(l+1)}_j + \tilde{\Phi}^{(l+1)}_{j-1} = \frac{1}{\tilde{D}}(\tilde{\Phi}^{(l+1/2)}_{1,j+1/2} - \tilde{\Phi}^{(l+1/2)}_{1,j-1/2}) + \tilde{\Phi}^{(l+1/2)}_{j+1} - 2\tilde{\Phi}^{(l+1/2)}_j + \tilde{\Phi}^{(l+1/2)}_{j-1} \ , \tag{16h}$$

$$\tilde{\Phi}^{(l+1)}_{1,1/2} = \tilde{\Phi}^{(l+1)}_{1,J+1/2} \ , \tag{16i}$$

$$0 = \frac{1}{J}\sum_{j=1}^{J}\tilde{\Phi}^{(l+1)}_j \ , \tag{16j}$$

$$\tilde{\phi}_k^{(l+1)} = \tilde{\phi}_k^{(l+1/2)} + \tilde{\Phi}_j^{(l+1)} - \tilde{\Phi}_j^{(l+1/2)} \ , \ \ 1 \leq j \leq J \ , \ \ k \in j \ . \tag{16k}$$

To simplify the Fourier ansatz, a new *relative* coordinate system is introduced [8]:

$$k = (j-1)p + r \ . \tag{17}$$

Here, k is the global fine cell index, j is the index of the coarse cell in which fine cell k resides, p is the number of fine cells per coarse cell, and r is the position of fine cell k within coarse cell j. With this coordinate system in place, we introduce the Fourier ansatz:

$$\tilde{\psi}_{k-1/2,m}^{(l+1/2)} = \omega^l a_{r,m} e^{i\Sigma_t \lambda x_j} \ , \tag{18a}$$

$$\tilde{\psi}_{k,m}^{(l+1/2)} = \omega^l b_{r,m} e^{i\Sigma_t \lambda x_j} \ , \tag{18b}$$

$$\tilde{\phi}_k^{(l+1/2)} = \omega^l B_r e^{i\Sigma_t \lambda x_j} \ , \tag{18c}$$

$$\tilde{\Phi}_j^{(l+1/2)} = \omega^l D e^{i\Sigma_t \lambda x_j} \ , \tag{18d}$$

$$\tilde{\Phi}_j^{(l+1)} = \omega^l F e^{i\Sigma_t \lambda x_j} \ , \tag{18e}$$

$$\tilde{\phi}_k^{(l+1)} = \omega^{l+1} G_r e^{i\Sigma_t \lambda x_j} \ . \tag{18f}$$

The fine-grid error coefficients are assumed to be periodic on the coarse grid, such that:

$$\tilde{\psi}_{(k+p)-1/2,m}^{(l+1/2)} = \left(\tilde{\psi}_{k-1/2,m}^{(l+1/2)}\right) e^{i\Sigma_t \lambda \Delta} = \omega^l a_{r,m} e^{i\Sigma_t \lambda (x_j + \Delta)} \ . \tag{19}$$

Inserting the ansatz into Eqs. (16) and simplifying, we obtain the following system of equations:

$$\begin{cases} \frac{\mu_m}{h}\left(a_{r+1,m} - a_{r,m}\right) + \Sigma_t b_{r,m} - \frac{\Sigma_s}{2} B_r = \frac{\Sigma_a}{2} G_r \ , & 1 \leq r < p \ , \\ \frac{\mu_m}{h}\left(a_{1,m} e^{i\Sigma_t \lambda \Delta} - a_{r,m}\right) + \Sigma_t b_{r,m} - \frac{\Sigma_s}{2} B_r = \frac{\Sigma_a}{2} G_r \ , & r = p \ , \end{cases} \tag{20a}$$

$$a_{1,m} = a_{1,m} e^{i\Sigma_t \lambda X} \ , \tag{20b}$$

$$\begin{cases} b_{r,m} = \left[\frac{1+\alpha_m}{2}\right] a_{r+1,m} + \left[\frac{1-\alpha_m}{2}\right] a_{r,m} \ , & 1 \leq r < p \ , \\ b_{r,m} = \left[\frac{1+\alpha_m}{2}\right] a_{1,m} e^{i\Sigma_t \lambda \Delta} + \left[\frac{1-\alpha_m}{2}\right] a_{r,m} & r = p \ , \end{cases} \tag{20c}$$

$$B_r = \sum_{m=1}^{M} w_m b_{r,m} \ , \tag{20d}$$

$$D = \frac{1}{p} \sum_{r=1}^{p} B_r \ , \tag{20e}$$

$$2(F-D)(\cos(\Sigma_t \lambda \Delta) - 1) = 3\Sigma_t \Delta \sum_{m=1}^{M} w_m \mu_m a_{1,m} (e^{i\Sigma_t \lambda \Delta} - 1) \ , \tag{20f}$$

$$\sum_{m=1}^{M} w_m \mu_m a_{1,m} = e^{i\Sigma_t \lambda X} \sum_{m=1}^{M} w_m \mu_m a_{1,m} \ , \tag{20g}$$

$$0 = \sum_{j=1}^{J} e^{i\Sigma_t \lambda x_j} \ , \tag{20h}$$

$$\omega G_r - B_r = (F - D) \ . \tag{20i}$$

From the boundary equations (20b) and (20g), we determine permissible values of the Fourier frequency λ for the discrete system:

$$\lambda_n = \frac{2n\pi}{\Sigma_t X} \ , \ \ 1 \leq n < J \ . \tag{21}$$

This set of Fourier frequencies automatically satisfies the normalization condition in Eq. (20h). Next, Eqs. (20d) and (20i) are used to eliminate F, D, and B_r in the remainder of Eqs. (20). We also define

$$c = \frac{\Sigma_s}{\Sigma_t} \ . \tag{22}$$

Inserting Eq. (22) and carrying out further simplification yields the following discrete system of equations:

$$\begin{cases} \frac{\mu_m}{\Sigma_t h} \left(a_{r+1,m} - a_{r,m}\right) + b_{r,m} - \frac{c}{2} \sum_{m'=1}^{M} w_{m'} b_{r,m'} - \frac{(1-c)}{2} G_r = 0 \ , & 1 \leq r < p \ , \\ \frac{\mu_m}{\Sigma_t h} \left(a_{1,m} e^{i\Sigma_t \lambda_n \Delta} - a_{r,m}\right) + b_{r,m} - \frac{c}{2} \sum_{m'=1}^{M} w_{m'} b_{r,m'} - \frac{(1-c)}{2} G_r = 0 \ , & r = p \ , \end{cases} \tag{23a}$$

$$\begin{cases} \left[\frac{1+\alpha_m}{2}\right] a_{r+1,m} + \left[\frac{1-\alpha_m}{2}\right] a_{r,m} - b_{r,m} = 0 \ , & 1 \leq r < p \ , \\ \left[\frac{1+\alpha_m}{2}\right] a_{1,m} e^{i\Sigma_t \lambda_n \Delta} + \left[\frac{1-\alpha_m}{2}\right] a_{r,m} - b_{r,m} = 0 & r = p \ , \end{cases} \tag{23b}$$

$$\sum_{m=1}^{M} w_m \left(E \mu_m a_{1,m} + b_{r,m}\right) - \omega G_r = 0 \ , \tag{23c}$$

where

$$E = \frac{3\Sigma_t \Delta}{2}\left[1 + \frac{i\sin(\Sigma_t \lambda_n \Delta)}{(\cos(\Sigma_t \lambda_n \Delta) - 1)}\right] . \tag{23d}$$

Eqs. (23) can be written in block matrix form [8]:

$$\begin{bmatrix} \mathbf{A} & \mathbf{B} \\ \mathbf{C} & -\omega\mathbf{I} \end{bmatrix} \begin{bmatrix} \mathbf{x} \\ \mathbf{y} \end{bmatrix} = \begin{bmatrix} \mathbf{0} \\ \mathbf{0} \end{bmatrix} . \tag{24}$$

Here $\mathbf{A}$ is a $2Mp \times 2Mp$ matrix containing the coefficients of $a_{r,m}$ and $b_{r,m}$ from Eqs. (23a) and (23b), $\mathbf{B}$ is a $2Mp \times p$ matrix composed of the coefficients of G_r from Eqs. (23a) and (23b), and $\mathbf{C}$ is a $p \times 2Mp$ matrix containing the coefficients of $a_{r,m}$ and $b_{r,m}$ from Eq. (23c). The final matrix $(-\omega\mathbf{I})$ is a $p \times p$ diagonal matrix containing the negative of the eigenvalues ω_r, which comprise the coefficients of G_r in Eqs. (23c). The size-$2Mp$ column vector $\mathbf{x}$ contains the $a_{r,m}$ and $b_{r,m}$ values, while the size-p column vector $\mathbf{y}$ contains the G_r values. To solve for the system eigenvalues ω_r, we follow the procedure outlined in [8]. The block matrix system is first decomposed:

$$\begin{bmatrix} \mathbf{A} & \mathbf{B} \\ \mathbf{C} & -\omega\mathbf{I} \end{bmatrix} = \begin{bmatrix} \mathbf{A} & \mathbf{0} \\ \mathbf{C} & \mathbf{I} \end{bmatrix} \begin{bmatrix} \mathbf{I} & \mathbf{A^{-1}B} \\ \mathbf{0} & -\mathbf{CA^{-1}B} - \omega\mathbf{I} \end{bmatrix} . \tag{25}$$

The determinant of the original system is then calculated using

$$\begin{vmatrix} \mathbf{A} & \mathbf{0} \\ \mathbf{C} & \mathbf{I} \end{vmatrix} \begin{vmatrix} \mathbf{I} & \mathbf{A^{-1}B} \\ \mathbf{0} & -\mathbf{CA^{-1}B} - \omega\mathbf{I} \end{vmatrix} = |\mathbf{A}||-\mathbf{CA^{-1}B} - \omega\mathbf{I}| = \mathbf{0} . \tag{26}$$

From inspection, the determinant of the original block matrix system is zero, while the determinant of matrix $\mathbf{A}$ is non-zero. Thus, we can infer that

$$|-\mathbf{CA^{-1}B} - \omega\mathbf{I}| = \mathbf{0} , \tag{27}$$

where $\mathbf{CA^{-1}B}$ and $\mathbf{I}$ are $p \times p$ matrices.

Using Eq. (27), the eigenvalues ω_r can be calculated numerically for $1 \leq r \leq p$ and permitted values of the discrete Fourier frequency, λ_n. Once the eigenvalues are known, the spectral radius ρ is determined using

$$\rho = \sup_{1 \leq n < J} \left(\sup_{1 \leq r \leq p} |\omega_r(\lambda_n)| \right) . \tag{28}$$

5. Application to MC-CMFD and S_N Surrogate

As a first test of the validity of the Fourier analysis, we compare its predictions to spectral radius estimates obtained from a "surrogate" discrete ordinates - CMFD (S_N-CMFD) code. The surrogate code treats the scattering source implicitly, as in the non-random MC-CMFD method. Instead of performing a fixed number of inner scattering source iterations per outer fission source iteration, the surrogate code performs as many inner scattering source iterations as is necessary to converge the scattering source to a very small tolerance. When run on a fine space-angle grid, the surrogate code should behave much like Monte Carlo in the limit as the number of histories approaches infinity. Thus, the spectral radius estimate produced using a fine space-angle grid should well-approximate the estimate using the Fourier analysis.

To determine a sufficiently fine space-angle grid, we performed a parametric study using the Fourier analysis script developed for this work. Values of the coarse-grid parameter p and angular order M were successively increased for a problem with fixed cross sections $\Sigma_t = 1$ cm^{-1}, $\nu\Sigma_f = 0.01$ cm^{-1}, and $\Sigma_s = 0.5$ cm^{-1}. The study was repeated twice, for coarse grids $\Delta = 1$ cm and $\Delta = 5$ cm. Resulting spectral radius estimates were then plotted as a function of the coarse-grid parameter and number of discrete angles. These plots are shown in Fig. (1).

In both cases, the spectral radius curve changes significantly when the number of discrete angles M is small, but becomes flat for $M \geq 16$. For the $\Delta = 1$ cm case, we see a large shift in the spectral radius estimate between the $p = 2$ and $p = 5$ curves, but for $p \geq 10$ the change in the spectral radius is small (on the order of 10^{-3}). For $\Delta = 5$ cm, the change in the spectral radius estimate becomes small for $p \geq 25$.

Based on this study, we opted to use $p = 50$ and the S_{32} quadrature set for our work. This particular discretization provided sufficient accuracy for the discrete approximation across a wide range of coarse grid sizes, while maintaining reasonable runtimes and memory demands for the Fourier analysis script. Due

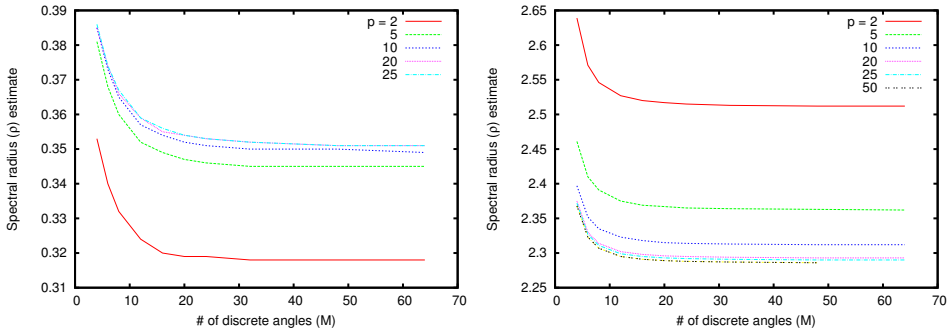

(a) $\Delta = 1$ cm (b) $\Delta = 5$ cm

Figure 1: **Discrete spectral radius estimate (ρ) as a function of angular order M and coarse-grid parameter p**

to the size of the block matrix system ($[2Mp + p] \times [2Mp + p]$), the spectral radius calculation becomes intractable for large values of M and p. While there is inevitably an error in the discrete results, this error should be small.

Next, in our direct MC-CMFD and surrogate S_N-CMFD simulations, we employed the following well-known spectral radius estimate:

$$\rho = \frac{||\Phi^{(l+1)} - \Phi^{(l)}||}{||\Phi^{(l)} - \Phi^{(l-1)}||} \, . \tag{29}$$

This expression requires estimates of Φ for three consecutive iterations, and is accurate for large values of l. For small values of ρ, this is slightly problematic for the surrogate S_N-CMFD simulations, since roundoff errors can significantly affect the accuracy of Eq. (29) after only a few iterations. It is much more problematic for the random MC-CMFD simulations, since the error in the fission source can quickly become reduced to the magnitude of the statistical errors.

Fortunately, small values of ρ, which are the most difficult to estimate, are not so interesting because the iteration method converges very rapidly. Larger values of ρ, closer to or greater than unity, are much more interesting, and for these Eq. (29) is more accurate.

The k-eigenvalue test problem considered in this paper is a homogeneous 50-centimeter slab with periodic boundaries. The total and fission cross sections

are fixed, while the scattering cross section takes one of four values. The coarse grid size varies between 1.0 and 12.5 mean free paths (mfp), keeping in mind that there must be an integer number of coarse cells. Numerical data for the problem are provided in Table 1.

Table 1: **Test Problem Specifications**

Σ_t (cm^{-1})	$\nu\Sigma_f$ (cm^{-1})	Σ_s (cm^{-1})	Δ (cm)
1.0	0.01	0.5, 0.75, 0.9, 0.99	1.0 - 12.5

For each coarse grid/scattering ratio combination, we calculate the theoretical spectral radius using $p = 50$ with the S_{32} Gauss-Legendre quadrature set. The numerical spectral radius is then estimated using our surrogate S_N-CMFD code. We reiterate that the discrete ordinates code performs many sweeps (inner iterations) to converge the scattering source to a tight tolerance (10^{-9}) before proceeding to the CMFD calculation, in order to mimic the non-random MC-CMFD method.

We were also able to estimate the spectral radius directly using a MC-CMFD code. Unfortunately, it is difficult to estimate ρ when the spectral radius is small (i.e. the fission source converges very quickly), because the magnitude of the fission source error becomes comparable to the stochastic error after very few cycles. Eq. (29) requires three cycles of flux data to numerically estimate the spectral radius; if ρ is small, the fission source error may already be small compared to the random error before an estimate can be calculated! Difficulties also occur when ρ is less than but close to unity; for these problems the random statistical errors in MC-CMFD can drive the barely-stable non-random MC-CMFD method unstable.

To estimate the MC-CMFD spectral radius numerically, the code was initialized with a random fission source guess. We then used Eq. (29) to generate a single value of ρ after the fourth cycle. This procedure was repeated for twenty-five independent simulations to obtain an average MC-CMFD ρ value, which is plotted along with its standard deviation in the subsequent figures. Evidence

from multiple trials shows that reasonably accurate estimates of ρ can only be obtained during the first few inactive cycles of each simulation (when the fission source error is larger than the random error). Because three cycles of coarse-grid fluxes are required to generate an estimate of ρ, the first value is not available until the end of the third iteration cycle. This estimate tends to be slightly biased (likely due to contamination from the initial guess), and we discard it. As a result, the earliest usable spectral radius estimate is calculated after the fourth iteration cycle.

In spite of these difficulties, we were able to calculate direct MC-CMFD spectral radius estimates for problems in which $0.5 < \rho < 0.98$. Again, if $\rho < 0.5$, the fission source converges too rapidly for Eq. (29) to become accurate. Also, if $\rho > 0.98$, then the random statistical errors in MC-CMFD can drive the barely-stable non-random MC-CMFD method unstable. For this reason, our direct estimates of ρ from MC-CMFD simulations become *very* noisy when $\rho \approx 1$.

But perhaps most importantly, our direct numerical simulations show that for a given scattering ratio, the Fourier analysis accurately predicts the coarse grid size at which the simulation becomes unstable.

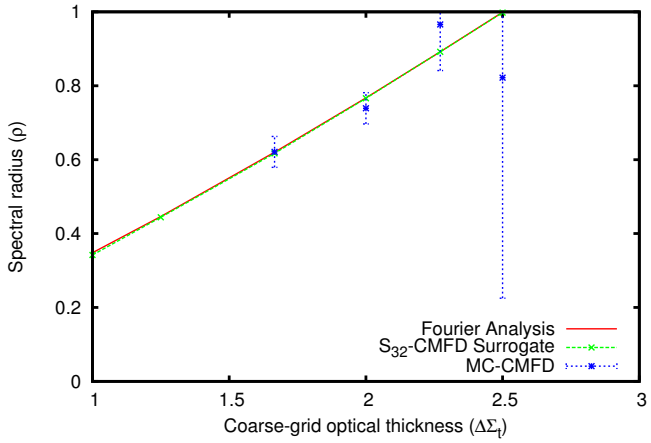

Figure 2: **Spectral radius (ρ) vs. coarse-grid optical thickness for $c = 0.5$**

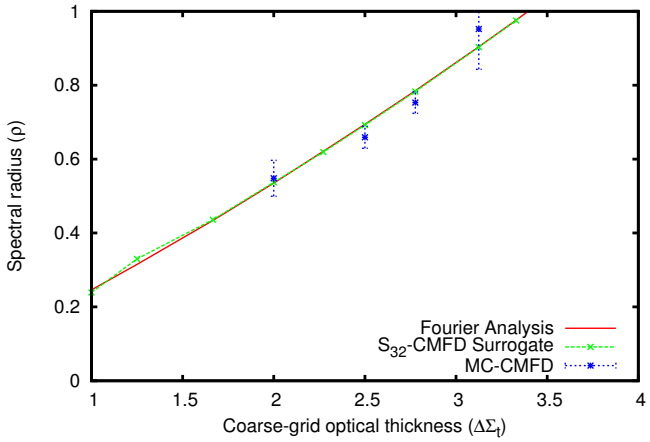

Figure 3: **Spectral radius (ρ) vs. coarse-grid optical thickness for c = 0.75**

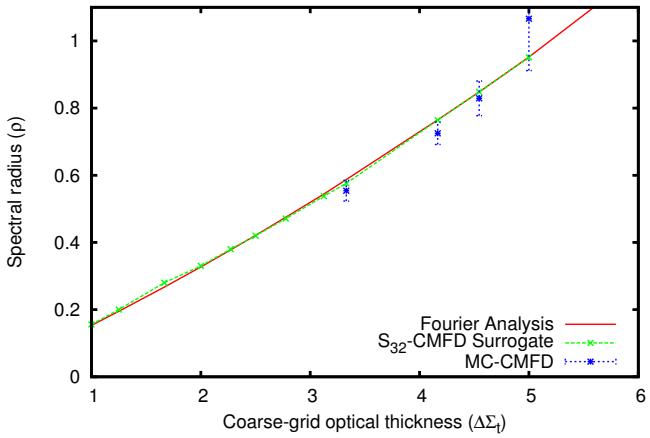

Figure 4: **Spectral radius (ρ) vs. coarse-grid optical thickness for c = 0.9**

Figs. (2) through (5) compare the theoretical, S_N-CMFD and MC-CMFD spectral radius results for $c = 0.5$, 0.75, 0.9 and 0.99, respectively. The S_N-CMFD spectral radius very closely matches the theoretical prediction for most cases, with the exception of problems in which the true spectral radius is very low. In these cases, the S_N-CMFD solution converges to machine precision too quickly to obtain an asymptotic ρ estimate.

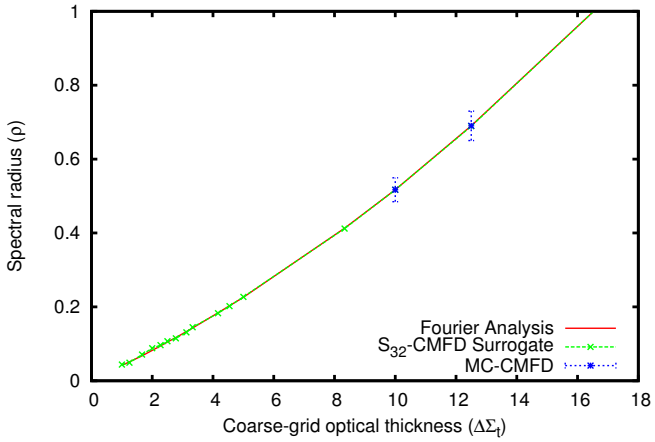

Figure 5: **Spectral radius (ρ) vs. coarse-grid optical thickness for c = 0.99**

There are several interesting trends in the MC-CMFD spectral radius data. First, the spectral radius increases monotonically as the coarse grid size increases. There appear to no be no coarse grid sizes between $\Delta = 1$ mfp and $\Delta = 12.5$ mfp for which the MC-CMFD method is stable for all values of the scattering ratio $0 \leq c < 1$, even in the limit as the number of particles becomes infinite.

Also, the Fourier analysis predicts that for a fixed coarse grid size, the spectral radius decreases (the method converges more rapidly) as the scattering ratio increases. This trend can be explained by examination of the MC-CMFD iteration strategy. As previously described, the Monte Carlo method treats scattering implicitly; the scattering source is converged entirely during the Monte Carlo sweep. If the scattering ratio is near unity, the Monte Carlo simulation does more "work" during a single iteration than it would for a low-scattering problem. This transfers a considerable amount of the convergence burden to the inner Monte Carlo sweep, which results in outer (CMFD) fission source convergence after very few cycles.

In addition, Figs. (2) - (5) show that the standard deviation of the MC-CMFD spectral radius estimate becomes large when $\rho \approx 1$. As the theoretical

spectral radius approaches unity, the fission source convergence rate becomes arbitrarily slow for the hypothetical case with no stochastic noise. Since our Monte Carlo simulations are necessarily run with a finite number of particles per cycle, our simulations have a non-negligible random error in quantities tallied during the Monte Carlo sweep. This additional error term can induce an instability in problems that are theoretically stable (in the infinite-particle limit). Therefore, spectral radius estimates from our CMFD-Monte Carlo code, for problems very near the predicted stability limit, tend to be noisy. This is especially obvious for the $c = 0.5$ case in Fig. (2).

When the MC-CMFD method is used in an unstable configuration, the coarse-grid flux shape develops a distinct cycle-to-cycle oscillation. An example of this is given in Fig. (6a), with a stable simulation in Fig. (6b) for comparison. The even-cycle fluxes in Fig. (6a) become increasingly tipped toward the left edge of the slab as the iteration cycles progress, while the odd-cycle fluxes increasingly tip toward the right. Eventually, the simulation will crash when the coarse-grid flux becomes negative, or when one or more coarse cells have no Monte Carlo data (we disabled negative flux detection to generate data for

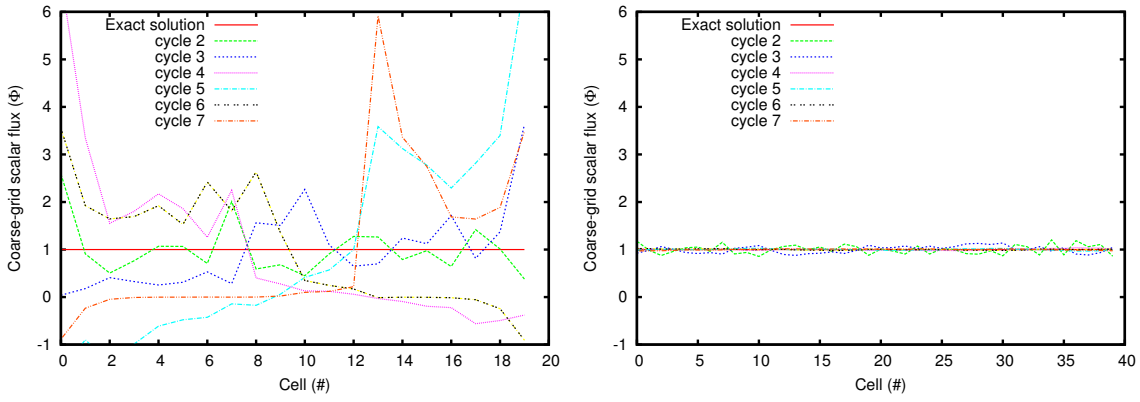

(a) $\Sigma_t \Delta = 2.5$ (b) $\Sigma_t \Delta = 1.25$

Figure 6: **Unstable vs. stable cycle-to-cycle coarse grid fluxes, $c = 0.5$**

Fig (6a)). We stress that the *only* difference between the results presented in

Fig. (6a) and Fig. (6b) is the coarse grid size; both simulations use the same random number seed, the same initial guess, the same number of particles per cycle, and the same cross sections.

Recent work [5] has attempted to mitigate oscillation in the MC-CMFD method by using Monte Carlo tallies from multiple cycles to form the CMFD system, a technique known as "accumulation." The effect of this approach is similar to running a larger number of Monte Carlo particles per iteration cycle. However, using tallies from more than one Monte Carlo cycle reintroduces some of the inter-cycle correlation normally suppressed by CMFD feedback. This complicates the iteration strategy by creating a need to reset Monte Carlo tallies periodically throughout the calculation. In essence, the tally accumulation technique does not address the underlying cause of the flux oscillation – a coarse grid size near or beyond the stability limit of the MC-CMFD method.

Finally, to better visualize the stability limit of the MC-CMFD method, we interpolated linearly between our Fourier analysis results to produce approximate constant-ρ curves. These curves are plotted as a function of coarse mesh size and scattering ratio, and are shown in Fig. (7). The phase space to the left of

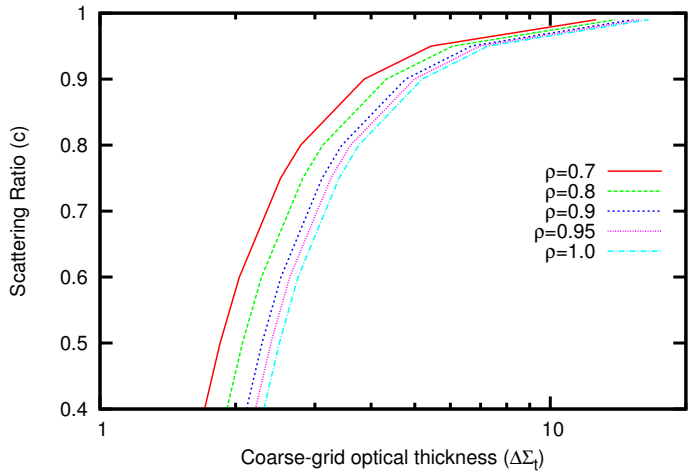

Figure 7: **Constant spectral radius curves as a function of $\Sigma_t\Delta$ and c**

the $\rho = 1.0$ line represents coarse grid/scattering ratio combinations for which the one-group planar non-random MC-CMFD method is stable. Conversely, the phase space to the right of the $\rho = 1.0$ line represents coarse grid/scattering ratio combinations for which the method is unstable. As the scattering ratio approaches unity, the non-random MC-CMFD stable grid size limit appears to tend towards infinity; for low scattering ratios ($c \leq 0.5$), the method becomes unstable for grids on the order of two mean free paths. We hypothesize that the presence of random error probably shifts these curves slightly to the left, but we cannot quantify this effect at present.

6. Discussion

In this work, a Fourier analysis is employed to predict the stability and convergence behavior of the MC-CMFD k-eigenvalue method, in the limit as the number of Monte Carlo particles approaches infinity. To carry out this analysis, (i) a sufficiently large number of Monte Carlo particles is used per cycle that random statistical effects can be ignored, (ii) the non-linear iteration scheme is linearized for a problem having a simple eigenfunction solution, and (iii) the linearized Monte Carlo problem is approximated with discrete ordinates on a fine space-angle grid, making it possible to solve a matrix system numerically for the spectral radius.

Theoretical predictions from the Fourier analysis compare very favorably with numerical results generated by a S_N-CMFD surrogate code, and also with a MC-CMFD code – provided that a large number of particles per cycle is used and the predicted spectral radius is not too small. When the predicted spectral radius is small ($\rho < 0.5$), the fission source converges too quickly to obtain an accurate estimate. However, the most interesting situations are ones in which the spectral radius ρ is close to or greater than unity. For these situations, the predictions of our Fourier analysis agree well with direct simulations.

The Fourier analysis and direct numerical simulations show that the spectral radius (i) increases monotonically as the coarse mesh optical thickness increases,

and (ii) decreases monotonically as the scattering ratio increases. Our results also show that the non-random MC-CMFD k-eigenvalue iteration becomes unstable when the coarse mesh exceeds a critical value (which, for the monoenergetic problem considered in this paper, depends on the scattering ratio c). These results imply that the MC-CMFD method should not be used for problems in which the non-random method is unstable. Fortunately, our results show that if the non-random MC-CMFD method is unstable, it can be stabilized by using a finer coarse grid. (Of course, this increases the cost of the low-order CMFD calculation.)

The analysis in this paper does not account for stochastic error, energy-dependent transport, or multidimensional transport. Thus, we cannot predict the effect of stochastic errors on convergence, nor can we quantitatively predict spectral radii for continuous energy, multigroup, or multidimensional problems. It is not clear whether our theory can be generalized to include stochastic errors. Conceptually, it is possible to extend the Fourier analysis to more complicated (multidimensional, multigroup) problems. However, the algebrac difficulties with even the simple 1-D, monoenergetic problems treated here are significant; extending this analysis to more complicated problems would be difficult. Fortunately, the work in this paper points to an alternate and more practical method for calculating spectral radii for realistic (multidimensional, multigroup) problems: use a surrogate S_N-CMFD code. Specifically, implement the non-random MC-CMFD algorithm in an S_N code and use the spectral radius estimates obtained from that. The 1-D results in this paper show excellent agreement between the Fourier analysis and the S_N-CMFD surrogate code, and there is no reason to think that this would not be true for more complicated problems. However, this task cannot be considered here.

In conclusion, we hope that the results derived in this paper will provide a more rigorous theoretical basis for applications of the MC-CMFD method. In particular, we hope that users of the method will be more aware of (previously unrecognized) stability issues, and that adequate steps will be taken to avoid simulations in which the non-random MC-CMFD method has a spectral radius

which is greater than, or too close to, unity.

7. Acknowledgement

We gratefully acknowledge support from the Consortium for Advanced Simulation of Light Water Reactors (www.casl.gov), an Energy Innovation Hub (http://www.energy.gov/hubs) for Modeling and Simulation of Nuclear Reactors under U.S. Department of Energy Contract No. DE-AC05-00OR22725.

References

[1] M. Lee, H. Joo, D. Lee, K. Smith, A feasibility study of cmfd acceleration in monte carlo eigenvalue calculation, in: Transactions of the Korean Nuclear Society Autumn Meeting, Gyeongju, Korea, 2009.

[2] M. Lee, H. Joo, D. Lee, K. Smith, Investigation of cmfd accelerated monte carlo eigenvalue calculation with simplified low dimensional multigroup formulation, in: Proceedings of PHYSOR 2010, Pittsburgh, Pennsylvania, 2010.

[3] M. Young, F. Brown, B. Kiedrowski, W. Martin, Coarse mesh finite difference in mcnp5, Tech. Rep. LA-UR-11-04384, Los Alamos National Laboratory (2011).

[4] M. Lee, H. Joo, D. Lee, K. Smith, Monte carlo reactor calculation with substantially reduced number of cycles, in: Proceedings of PHYSOR 2012, Knoxville, Tennessee, 2012.

[5] M. Lee, H. Joo, D. Lee, K. Smith, Coarse mesh finite difference formulation for accelerated monte carlo eigenvalue calculation, Annals of Nuclear Energy 65 (2014) 101.

[6] P. Romano, et al., Openmc: a state-of-the-art monte carlo code for research and development, Annals of Nuclear Energy.

[7] M. Adams, E. Larsen, Fast iterative methods for discrete-ordinates particle transport calculations, Progress in Nuclear Energy 40 (2002) 3.

[8] E. Larsen, B. Kelley, The relationship between the coarse-mesh finite difference and the coarse-mesh diffusion synthetic acceleration methods, Nuclear Science and Engineering 178 (2014) 1.

[9] K. Smith, J. Rhodes, Full-core, 2-d, lwr core calculations with casmo-4e, in: Proceedings of PHYSOR 2002, Seoul, Korea, 2002.

[10] D. Lee, T. Downar, Y. Kim, Convergence analysis of the nonlinear coarse-mesh finite difference method for one-dimensional fixed-source neutron diffusion problem, Nuclear Science and Engineering 147 (2004) 127.

[11] S. Hong, K.-S. Kim, J. Song, Fourier convergence analysis of the rebalance methods for discrete ordinates transport equations in eigenvalue problems, Nuclear Science and Engineering 164 (2010) 33.